Molecular dynamics simulation study of a polymer droplet transport over an array of spherical nanoparticles

Anish Thomas, Nikolai V. Priezjev*

Department of Mechanical and Materials Engineering, Wright State University, Dayton, OH 45435, United States

ABSTRACT

The dynamic behavior of a partially wetting polymer droplet driven over a nanostructured interface is studied using molecular dynamics simulations. We consider the bead-spring model to represent a polymeric liquid that partially wets a rough surface composed of a periodic array of spherical particles. It is shown that at sufficiently small values of the external force, the droplet remains pinned at the particles' surface, while above the threshold, its motion consists of alternating periods of pinning and rapid displacements between neighboring particles. The latter process involves large periodic variation of the advancing and receding contact angles due to attachment and detachment of the contact line. Finally, upon increasing external force, the droplet center of mass is displaced steadily but the oscillation amplitude of the receding contact angle as well as the maximum contact angle hysteresis remain relatively unaffected.

1. Introduction

The development of nanofabrication techniques is important for manufacturing the so-called *superhydrophobic* surfaces that possess liquid-repellent and self-cleaning properties [1]. The main design principle behind such surfaces is to introduce small-scale surface asperities that can keep the liquid interface suspended above the substrate and allow for the formation of trapped air pockets, thus reducing the liquid-solid contact area [2,3]. This situation is commonly referred to as the Cassie-Baxter state [4], whereas the case of a full penetration of a liquid into a rough surface is called the Wenzel state [5]. As a result, liquids in contact with superhydrophobic surfaces typically exhibit large contact angles, relatively small contact angle hysteresis, and reduced hydrodynamic friction. The enhanced slip properties also offer a more precise control of liquid flow in microfluidic and nanofluidic channels [6,7]. In particular, it was recently shown that the effective slip length for liquid flows over substrates with mixed boundary conditions can be accurately computed using either continuum or atomistic simulations, provided that the length scales of surface textures are larger than the molecular size [8–11].

In recent years, the wetting and flow properties of liquid droplets over nanotextured surfaces were examined using molecular dynamics simulations [12–29]. In the absence of external forces, the stability of the Wenzel or Cassie-Baxter states depends on the height of surface pillars, their surface fraction, and the intrinsic contact angle

[13,16,18,21]. In turn, the Cassie-to-Wenzel wetting transition at pillar-arrayed surfaces and subsequent spreading of the liquid can be facilitated by applying a sufficiently large electric field [20,22]. Furthermore, under an external force parallel to nano-pillared superhydrophobic surface, the advancing and receding contact lines of a water droplet are displaced in discrete steps, and the partially wetting droplet effectively rolls above the pillar tips [27,28]. More recently, it was shown that directed droplet motion along a hydrophobic stripe can be generated by periodic vibration of a substrate with asymmetric corrugations, and the droplet velocity follows a power-law dependence on the vibration period [29]. However, despite extensive efforts, the exact mechanisms of the contact line displacement, variation of the advancing and receding contact angles, and neck formation during pinning of a partially wetting droplet at nanostructured surfaces remain not fully understood.

In this paper, molecular dynamics simulations are carried out to investigate the effects of an external force and wettability on the displacement of a polymer droplet over a smooth substrate covered by periodically arranged spherical nanoparticles. It will be shown that below the threshold force, the partially wetting droplet remains pinned at the particles' surface, while at larger values of the external force, the droplet motion becomes intermittent and involves rapid displacements separated by periods of pinning. The process of attachment and detachment from the particle surface is associated with large variation of the advancing and receding contact angles. Interestingly, the maximum

---

* Corresponding author.
  E-mail address: nikolai.priezjev@wright.edu (N.V. Priezjev).

value of the contact angle hysteresis remains rather insensitive to the external force.

The rest of the paper is structured as follows. The details of the molecular dynamics simulation model and parameter values are given in the next section. The description of the fitting procedure for the droplet shape, examples of the droplet profiles at structured interfaces, and the time dependence of the droplet displacement as well as the variation of the advancing and receding contact angles are presented in Sec. 3. The last section contains a brief summary of the results.

2. Molecular dynamics simulations

In our study, a liquid droplet consists of 880 000 atoms interacting via the Lennard-Jones (LJ) potential. More specifically, any two atoms interact via the truncated LJ potential:

$$V_{LJ}(r) = 4\varepsilon \left[\left(\frac{\sigma}{r} \right)^{12} - \left(\frac{\sigma}{r} \right)^6 \right], \tag{1}$$

where the parameters ε and σ describe the energy and length scales of the liquid phase. The interaction between solid and liquid atoms is also described by the LJ potential with the parameters ε_{sp} (measured in units of ε) and $\sigma_{sp} = \sigma$. To speed up simulations, the cutoff radius $r_c = 2.5\sigma$ is used for all types of interactions. The equations of motion were solved using the velocity Verlet integration algorithm [30] with the time step $\triangle t_{MD} = 0.005\tau$, where $\tau = \sigma\sqrt{m/\varepsilon}$ is the LJ time. The molecular dynamics simulations were carried out using the LAMMPS parallel code [31].

In addition to the LJ interaction, liquid monomers are connected to form short chains (10 monomers per chain) via the FENE (finitely extensible nonlinear elastic) potential:

$$V_{FENE}(r) = -\frac{k}{2} r_o^2 \ln[1 - r^2/r_o^2], \tag{2}$$

with the parametrization $k = 30\varepsilon\sigma^{-2}$ and $r_o = 1.5\sigma$ [32]. Thus, the neighboring atoms within a chain interact via the LJ and FENE potentials, which effectively yields a harmonic potential that prevents polymer chains from unphysical crossing each other [32]. The temperature of the liquid phase, $T = 1.0\varepsilon/k_B$, was regulated via the Nosé-Hoover thermostat applied along the $\hat{y}$ direction (perpendicular to the droplet direction of motion). Here, k_B is the Boltzmann constant.

The polymer droplet is initially placed in contact with a composite substrate, which consists of an array of 10 spherical particles rigidly attached to a stationary solid plane, as shown in Fig. 1. The solid plane consists of 22 000 atoms arranged on a square lattice within the xy plane with lateral dimensions $440\sigma \times 50\sigma$. The atoms in the solid plane do not interact with each other and they are rigidly fixed to the lattice sites. Next, each spherical particle is composed of 4000 atoms uniformly distributed on a surface of a sphere with the radius $R = 17.8\sigma$. The areal density of atoms in the solid plane and spherical particles is $1.0\sigma^{-2}$. In our setup, the atoms on the surface of spherical particles do not interact with each other but the interaction energy between liquid monomers and particle atoms is controlled by the parameter ε_{sp} (measured in units of ε).

The preparation procedure involved a thermal equilibration of the polymeric liquid starting from the crystal phase. Periodic boundary conditions were imposed along the $\hat{x}$ and $\hat{y}$ directions, while the system is open along the $\hat{z}$ direction (perpendicular to the solid plane). After the initial equilibration, the liquid droplet was gradually displaced towards the composite substrate and further allowed to equilibrate in a partially wetting state at a given value of ε_{sp}. The droplet motion along the $\hat{x}$ direction was induced by a constant force, f_x, applied on each monomer. It should be noted that the force of gravity was not included in our study.
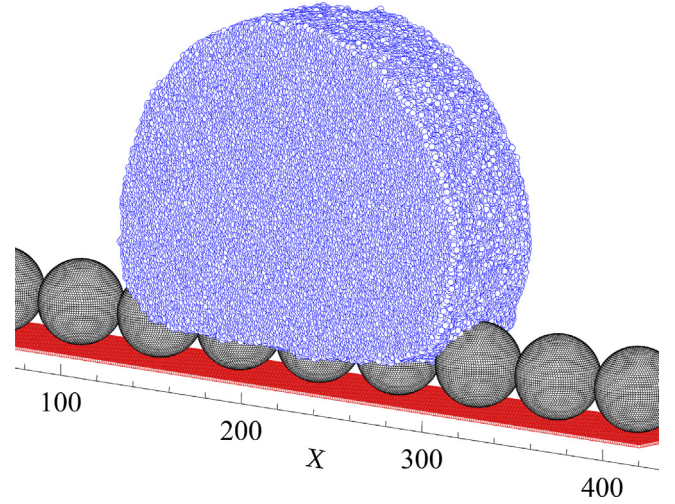

Fig. 1. An instantaneous snapshot of the liquid droplet that consists of 88 000 polymer chains (10 monomers per chain) and resides on the array of spherical particles rigidly attached to the solid substrate. The atoms are not shown to scale. The interaction energy between liquid monomers and particle atoms is $\varepsilon_{sp} = 0.6\varepsilon$. The external force $f_x = 0.00004\varepsilon/\sigma$ is applied on each monomer.

3. Results

It is well realized that the wetting properties of structured interfaces depend sensitively on a number of factors, *i.e.*, the areal density and shape of the surface texture, the surface energy, and the surface tension at the liquid-vapor interface [33]. In the present study, the surface roughness is introduced via an array of spherical particles, and the liquid is confined into a narrow slab with periodic boundary conditions to access larger droplet sizes. In turn, the liquid consists of short, flexible polymer chains in order to enhance surface tension and, thus, reduce evaporation from the liquid interface. The examples of droplet snapshots in contact with the periodic array of particles are displayed in Fig. 2 for selected values of the interaction energy between the liquid monomers and particle atoms. It can be seen that the droplet shape varies from nearly circular for $\varepsilon_{sp} = 0.2\varepsilon$ to semicircular for $\varepsilon_{sp} = 0.6\varepsilon$. In the latter case, the linear size of the droplet along the $\hat{x}$ direction is about 180σ. Taking $\sigma = 0.5$ nm, the typical size of the droplet is about 90 nm and the sphere radius is ≈ 9 nm.

We next describe the fitting procedure used to obtain the droplet profiles and apparent contact angles. The difficulty in computing the position of the liquid interface from instantaneous configuration of monomers arises due to thermal fluctuations that result in a finite width of the interface. Therefore, the computational domain was divided into narrow slices (with thickness of 1.0σ) parallel and perpendicular to the solid wall. In each slice, the local density of liquid monomers was computed and the location of the droplet interface was determined at half the density of liquid monomers in the center of the droplet. An example of the two-dimensional droplet interface profile is presented in Fig. 3. In general, the definition of the apparent contact angle at the atomic scale can be ambiguous. In our setup, we choose a plane located on the distance $2R$ from the solid wall as a reference for computing the apparent contact angles (see the horizontal black line in Fig. 3). Next, the front and back portions of the interface were obtained via the 4-th order polynomial fit, and the tangent at the intersection with reference plane was computed using the first 10 data points. The accuracy of this procedure was tested by trial and error for various shapes of the droplet during its motion over an array of particles. In what follows, we define the advancing, θ_a, and receding, θ_r, contact angles at the front and back of the droplet with respect to the direction of the external force.

The dependence of the apparent (static) contact angle as a function of the interaction energy between sphere atoms and droplet monomers,
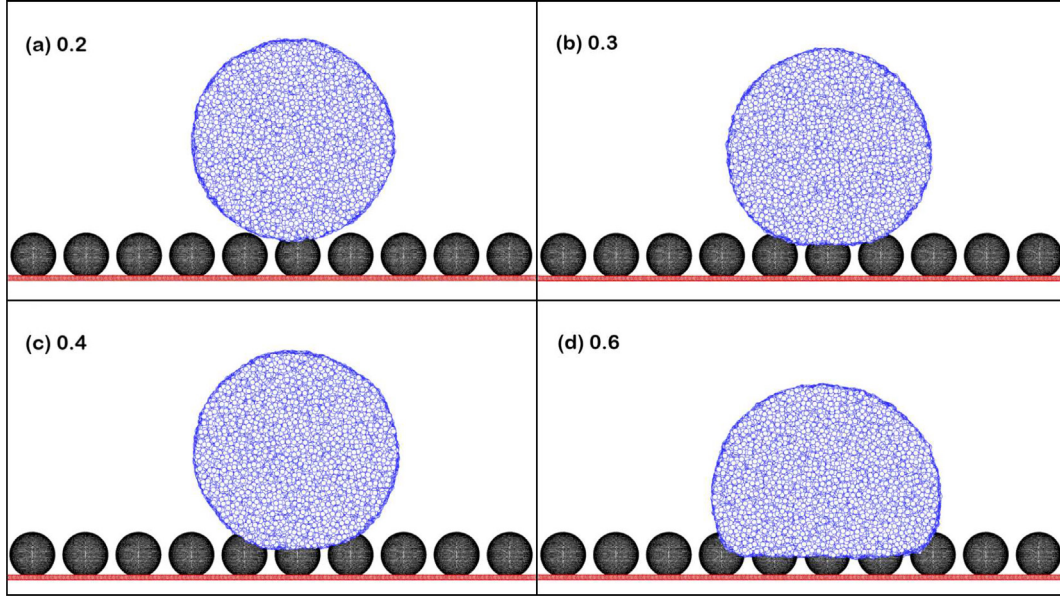
Fig. 2. The side view of polymer droplets in contact with solid particles for the surface energies (a) $\varepsilon_{sp} = 0.2\varepsilon$, (b) $\varepsilon_{sp} = 0.3\varepsilon$, (c) $\varepsilon_{sp} = 0.4\varepsilon$, and (d) $\varepsilon_{sp} = 0.6\varepsilon$.
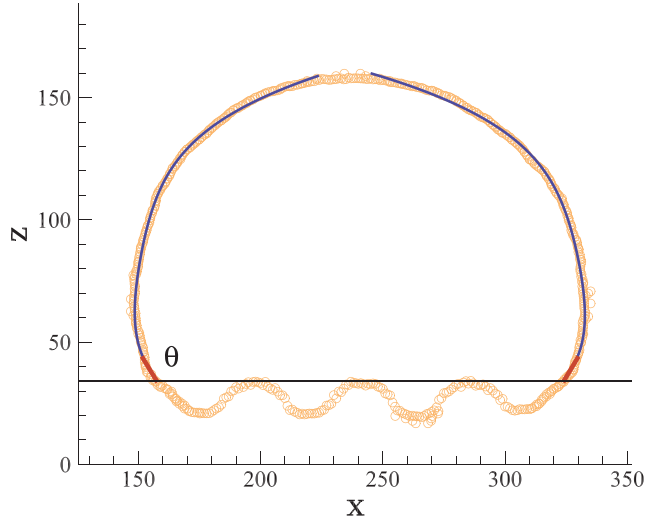

Fig. 3. An example of the droplet interface (orange circles) computed from the spatial variation of the local density profiles (see text for details) for $\varepsilon_{sp} = 0.6\varepsilon$ and $f_x = 0$. The horizontal black line denotes the reference plane above the tips of spherical particles. The blue curves indicate the 4-th order polynomial fit, and the red lines denote the local tangents to the polymer interface used to compute the apparent contact angles.
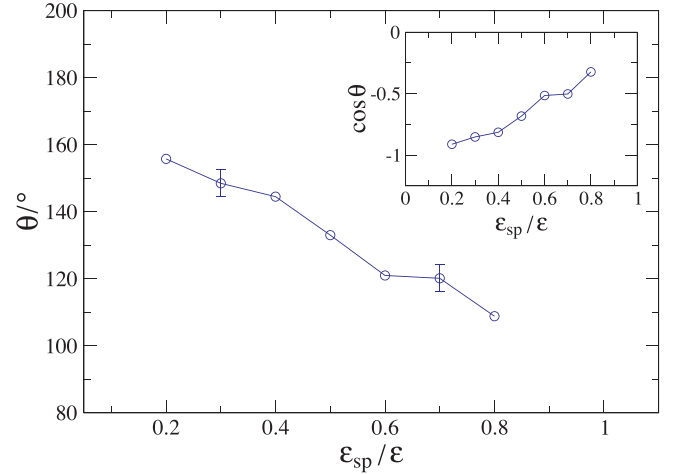

Fig. 4. The apparent contact angle for the droplet suspended on an array of spherical particles as a function of the interaction energy between sphere atoms and liquid monomers. The same data are replotted in the inset as $\cos\theta(\varepsilon_{sp})$.
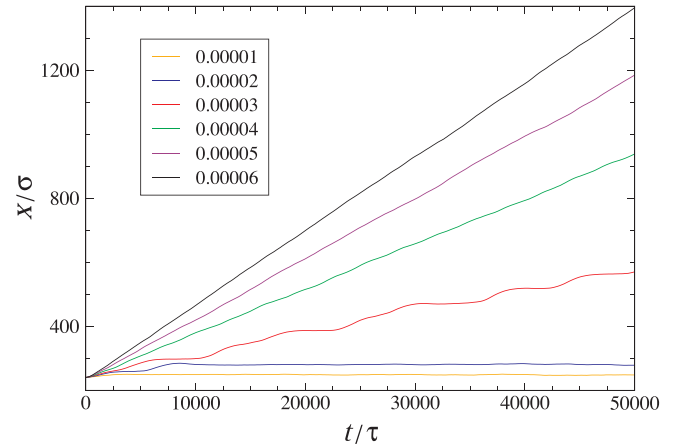

Fig. 5. The time dependence of the droplet center of mass for the indicated values of the external force, f_x (in units ε/σ). The interaction energy between sphere atoms and liquid monomers is $\varepsilon_{sp} = 0.6\varepsilon$.

$\varepsilon_{sp}/\varepsilon$, is shown in Fig. 4 in the absence of the external force. As is evident, the contact angle decreases monotonically with increasing surface energy; however, the droplet remains in a partially wetting state for $\varepsilon_{sp} \leqslant 0.8\varepsilon$. Note that these results are obtained for a specific areal fraction, i.e., $\phi_S = 10\pi R^2/A \approx 0.48$, where $A = 50 \times 440\sigma^2$ is the area of the solid plane, and $R = 18.3\sigma$ is the radius of a sphere with the excluded volume of atoms of size σ. In the recent study, it was shown that the critical pressure, below which a polymer film remains suspended on an array of spherical particles with a similar areal fraction, can be equally well estimated by MD simulations and numerical minimization of the interfacial energy [34]. We comment also that the local contact angle of a polymer (10-mers) droplet residing on a flat solid plane with the density of $1.0\sigma^{-2}$ was evaluated previously as a function of the surface energy [34].

We next study the droplet displacement under external force applied to each monomer along the $\hat{x}$ direction. Fig. 5 shows the time
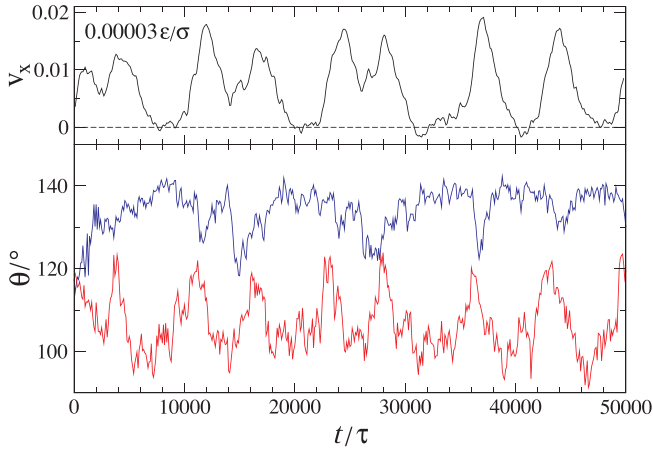
Fig. 6. The velocity of the center of mass (in units σ/τ) as a function of time when $f_x = 0.00003\varepsilon/\sigma$ (the upper panel). The horizontal dashed line indicates $v_x = 0$. The advancing (blue curve) and receding (red curve) contact angles during $50\,000\tau$ (the lower panel). The surface energy is $\varepsilon_{\rm sp} = 0.6\varepsilon$.

dependence of the droplet center of mass for the indicated values of the external force. In all cases, the droplet is initially at equilibrium with the structured interface, and the external force, f_x, is suddenly applied to each monomer at time $t = 0$. It can be clearly observed that at small values of the force, $f_x \leqslant 0.00002\varepsilon/\sigma$, the droplet is initially displaced on the distance between neighboring spheres but it remains pinned during the time interval $50\,000\tau$. At the larger value of the external force, $f_x = 0.00003\varepsilon/\sigma$, the droplet becomes temporarily pinned at the particle surface and then rapidly moves along the array of particles. Upon further increasing force, the motion becomes more steady although small fluctuations remain noticeable in the cases $f_x = 0.00004\varepsilon/\sigma$ and $0.00005\varepsilon/\sigma$. Finally, when $f_x = 0.00006\varepsilon/\sigma$, the droplet is displaced linearly on the distance of about 6 times its size during $50\,000\tau$.

An additional insight into the droplet dynamics can be gained by analyzing the time dependence of the advancing and receding contact angles. In Figs. 6–8, the variation of the advancing and receding contact angles as well as the velocity of the center of mass are reported for selected values of the external force. In the case $f_x = 0.00003\varepsilon/\sigma$ shown in Fig. 6, it can be observed that droplet dynamics consists of alternating periods of rapid motion and temporal pinning at the surface of spheres. In general, the maximum of the center of mass velocity correlates well with the abrupt changes in the contact angles. Namely, the
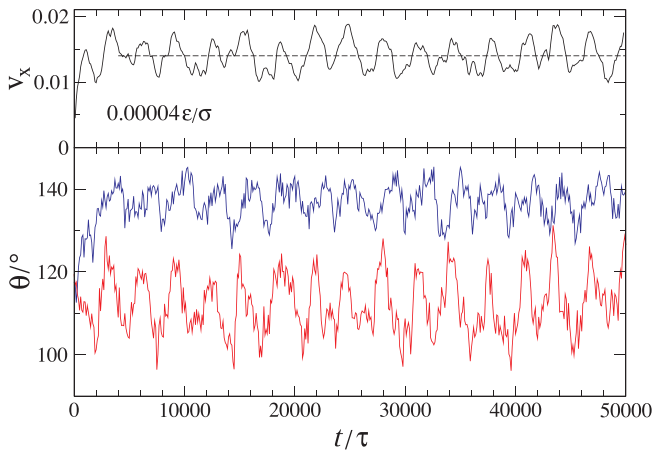

Fig. 7. The center of mass velocity (in units σ/τ) as a function of time when $f_x = 0.00004\varepsilon/\sigma$ (the upper panel). The dashed line denotes the average velocity $v_x = 0.014\sigma/\tau$. The interaction energy between sphere atoms and droplet monomers is $\varepsilon_{\rm sp} = 0.6\varepsilon$. The time dependence of the advancing (blue curve) and receding (red curve) contact angles for $f_x = 0.00004\varepsilon/\sigma$ (the lower panel).
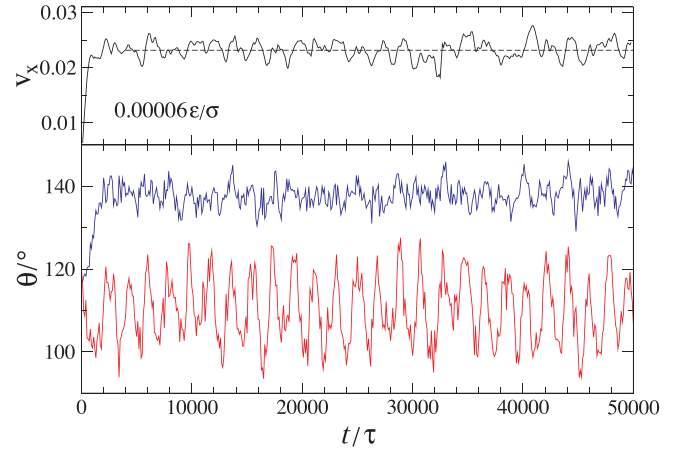

Fig. 8. The upper panel shows the velocity of the center of mass (in units σ/τ) versus time for $f_x = 0.00006\varepsilon/\sigma$. The average velocity $v_x = 0.023\sigma/\tau$ is indicated by the dashed line. The surface energy is $\varepsilon_{\rm sp} = 0.6\varepsilon$. The lower panel displays the advancing (blue curve) and receding (red curve) contact angles as a function of time.

advancing contact angle is reduced, while the receding angle increases during transient motion along the array of spherical particles. Interestingly, one can also notice in Fig. 6 that the center of mass velocity occasionally becomes negative between successive displacements, indicating a slight oscillatory movement due to surface tension forces. In addition, the contact angle hysteresis varies from $\theta_a - \theta_r \approx 45°$ during periods of pinning to nearly zero during rapid displacements (see Fig. 6).

Fig. 7 shows the droplet velocity and the contact angles for a larger value of the external force $f_x = 0.00004\varepsilon/\sigma$. It can be seen that after the first jump, the droplet is steadily propelled with the average velocity $v_x = 0.014\sigma/\tau$ along the array of particles, and the amplitude of oscillations of the contact angles is reduced, so that the advancing contact angle is greater than the receding angle. The period of the velocity and contact angles variation is determined by the center of mass velocity and the distance between neighboring spheres. Note also that the maximum value of the contact angle hysteresis is nearly the same as in the case $f_x = 0.00003\varepsilon/\sigma$, i.e., $\theta_a - \theta_r \approx 45°$.

Furthermore, when the external force is $f_x = 0.00006\varepsilon/\sigma$, the average droplet velocity becomes larger, $v_x = 0.023\sigma/\tau$, and the fluctuations of v_x and θ_a are significantly reduced, as shown in Fig. 8. Notice, however, that the oscillation amplitude of the receding contact angle remains relatively large and it is comparable to the cases $f_x = 0.00003\varepsilon/\sigma$ and $0.00004\varepsilon/\sigma$. In general, the maximum contact angle hysteresis remains rather insensitive to the value of the external force, as shown in Figs. 6–8. In the previous MD study, the values of surface tension $\gamma = 0.85\varepsilon/\sigma^2$ and viscosity $\eta = 11.1\,m/\tau\sigma$ were computed for a thin polymer film of bead-spring chains (10-mers) at $T = 1.0\varepsilon/k_B$ and zero pressure [35]. These values were used to estimate the capillary number $Ca = \eta v_x/\gamma \approx 0.3$, which indicates that the droplet motion is dominated by surface tension for all values of the external force, $f_x \leqslant 0.00006\varepsilon/\sigma$, considered in the present study. For reference, the typical value of the Weber number is $We = \rho v_x^2 \ell/\gamma \approx 0.1$, where $\ell \approx 180\sigma$ is the droplet size and $v_x = 0.023\sigma/\tau$.

The processes of attachment and detachment of the polymer interface at the particles' surface are visualized in Figs. 9 and 10. The snapshots of the droplet shape are taken at selected time intervals after the external force $f_x = 0.00003\varepsilon/\sigma$ is applied at $t = 0$. The displacement of the center of mass for these cases is denoted by the red curve in Fig. 5. It can be observed in Fig. 9 (b-g) that the advancing interface remains effectively suspended in front of the second rightmost particle during the extended time interval of about $\Delta t = 5000\tau$, while the advancing contact angle is the largest, $\theta_a \approx 140°$, when $t = 9000\tau$ (see
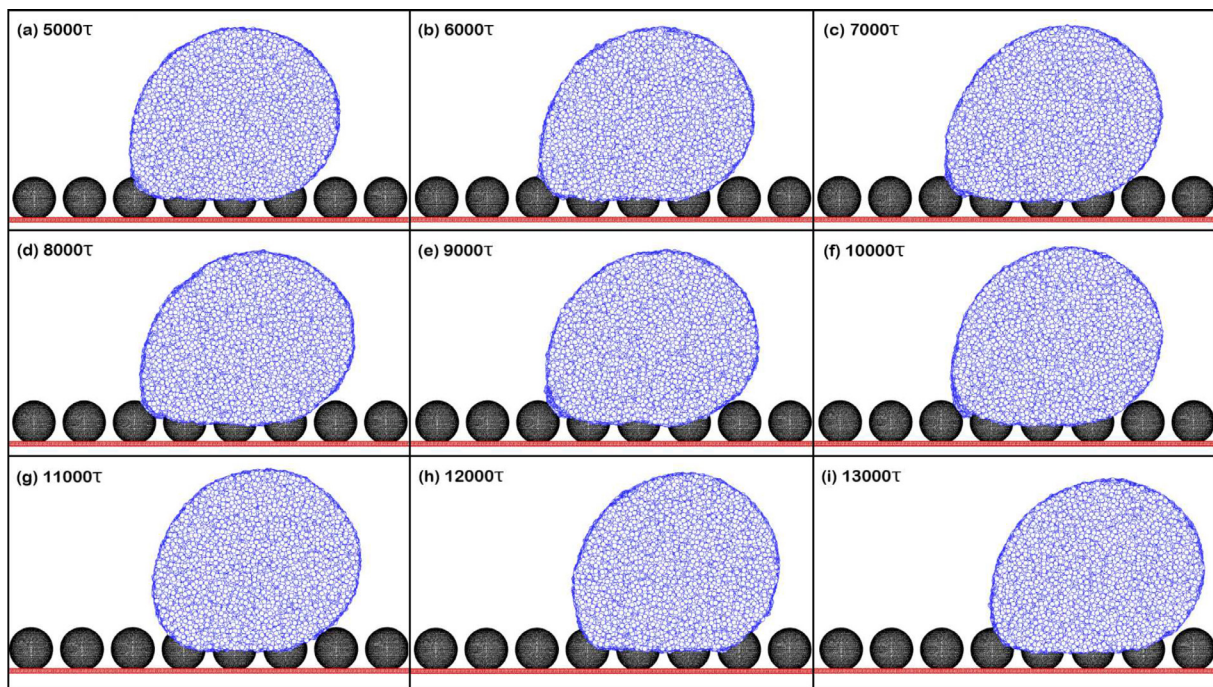
Fig. 9. The sequence of snapshots illustrating the advancement of the droplet front interface over the array of particles. The external force is $f_x = 0.00003\,\varepsilon/\sigma$ and the surface energy is $\varepsilon_{sp} = 0.6\,\varepsilon$. The time is measured after f_x is applied at $t = 0$ (see the red curve in Fig. 5).

Fig. 6). Furthermore, the sequence of snapshots in Fig. 10(a–g) shows the time evolution of the circular contact line at the third particle which temporarily restrains the droplet motion. Notice in Fig. 10(e–g) that a narrow neck is formed above the particle surface, followed by rapid detachment of the polymer interface and displacement of the whole droplet along the substrate. These results suggest that one of the factors determining the pinning time is the shape of surface texture; and, thus, the droplet motion along the surface can be controlled by introducing shape anisotropy of the surface-attached particles.

A quantitative description of the attachment and detachment of the droplet interface on the surface of a spherical particle can be obtained by computing the number of fluid monomers in contact with surface atoms. More specifically, at any instant of time, we identified fluid monomers that are located within the distance 1.5σ from the position of an atom of a particular sphere. The results are shown in Fig. 11 for the case $\varepsilon_{sp} = 0.6\,\varepsilon$ and $f_x = 0.00003\,\varepsilon/\sigma$. As is evident, the number of
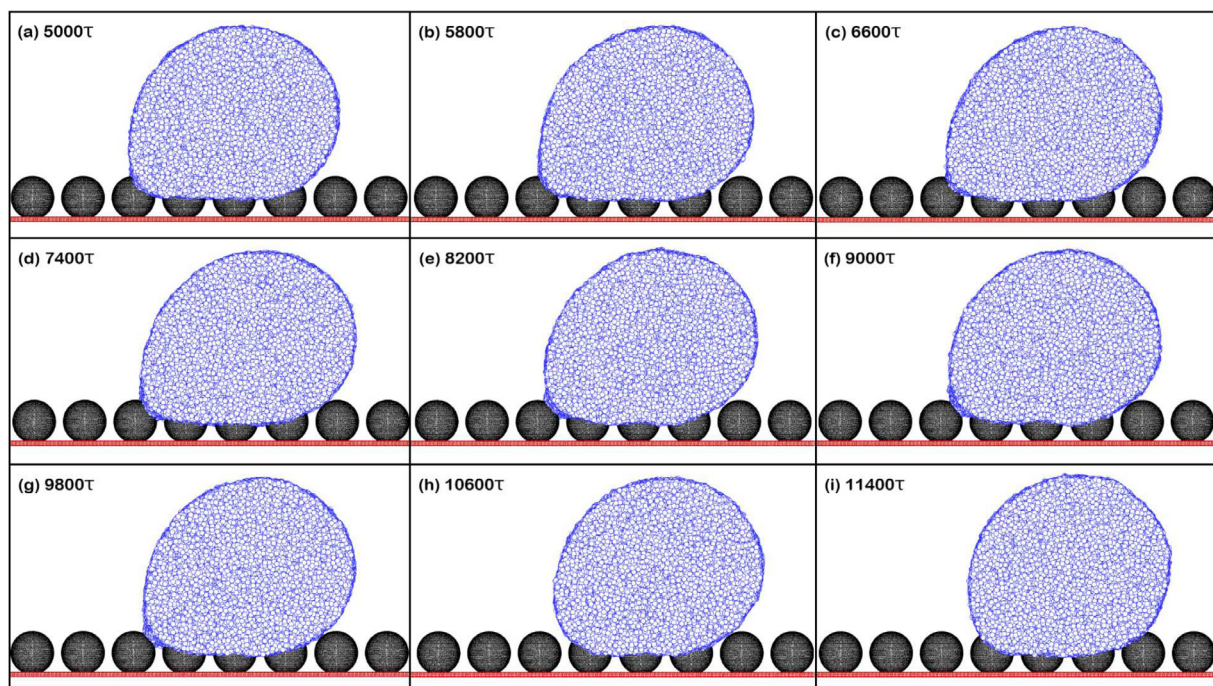

Fig. 10. The process of detachment of the receding contact line from the particle surface for the indicated time intervals after the external force $f_x = 0.00003\,\varepsilon/\sigma$ is applied on each monomer. The same data as in Fig. 5 (the red curve) and in Fig. 6. (For interpretation of the references to colour in this figure legend, the reader is referred to the web version of this article.)
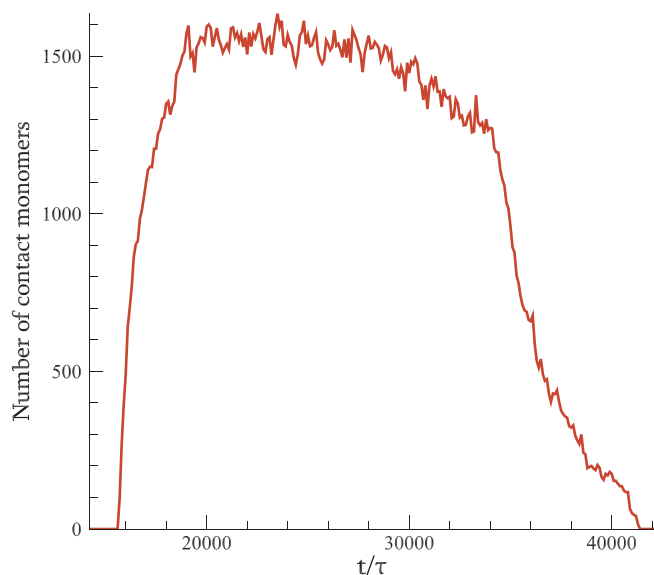
Fig. 11. The time dependence of the number of fluid monomers in contact with the surface of a spherical particle during droplet motion under the external force $f_x = 0.00003\varepsilon/\sigma$.

monomers in contact with one sphere first increases rapidly, then saturates to a quasi-plateau, followed by a slow decay. The sharp increase in the number of contact monomers corresponds to a rapid advancement of the droplet interface during step-like motion of the center of mass (see the red curve in Fig. 5). In turn, the plateau level represents about half of the surface area in contact with the liquid during droplet sliding along the substrate. Finally, the relatively slow decrease in the number of contact monomers describes the detachment of progressively narrowing neck that temporarily pins the whole droplet.

4. Conclusions

In summary, the dynamics of a polymer droplet driven over a nanostructured interface composed of an array of spherical particles was investigated using large-scale molecular dynamics simulations. The areal density of nanoparticles and the interaction energy between solid atoms and liquid monomers was adjusted to form a partially wetting droplet with the apparent contact angle greater than 90° at mechanical equilibrium. It was shown that the polymer droplet remains pinned at the surface of nanoparticles at sufficiently small values of the external force. Above the threshold force, the droplet moves intermittently along the interface via successive rapid displacements and periods of pinning. The process of attachment and detachment at the particles' surface causes significant distortion of the droplet shape quantified via advancing and receding contact angles. With increasing external force, the variation of the advancing contact angle is reduced, whereas the oscillation amplitude of the receding contact angle and the maximum contact angle hysteresis remain nearly unchanged.

Declaration of Competing Interest

The authors declare that they have no known competing financial interests or personal relationships that could have appeared to influence the work reported in this paper.

Acknowledgments

References

[1] E.K. Sam, D.K. Sam, X. Lv, B. Liu, X. Xiao, S. Gong, W. Yu, J. Chen, J. Liu, Recent development in the fabrication of self-healing superhydrophobic surfaces, Chem. Eng. 373 (2019) 531.

[2] J. Jeevahan, M. Chandrasekaran, G.B. Joseph, R.B. Durairaj, G. Mageshwaran, Superhydrophobic surfaces: a review on fundamentals, applications, and challenges, J. Coat. Technol. Res. 15 (2018) 231.

[3] P. Nguyen-Tri, H.N. Tran, C.O. Plamondon, L. Tuduri, D.-V.N. Vo, S. Nanda, A. Mishra, H.-P. Chao, A.K. Bajpai, Recent progress in the preparation, properties and applications of superhydrophobic nano-based coatings and surfaces: a review, Prog. Organ. Coat. 132 (2019) 235.

[4] A.B.D. Cassie, S. Baxter, Wettability of porous surfaces, Trans. Faraday Soc. 40 (1944) 546.

[5] R.N. Wenzel, Resistance of solid surfaces to wetting by water, Ind. Eng. Chem. 28 (1936) 988.

[6] O.I. Vinogradova, A.L. Dubov, Superhydrophobic textures for microfluidics, Mendeleev Commun. 22 (2012) 229.

[7] T. Lee, E. Charrault, C. Neto, Interfacial slip on rough, patterned and soft surfaces: a review of experiments and simulations, Adv. Colloid Interface Sci. 21 (2014) 210.

[8] N.V. Priezjev, A.A. Darhuber, S.M. Troian, Slip behavior in liquid films on surfaces of patterned wettability: comparison between continuum and molecular dynamics simulations, Phys. Rev. E 71 (2005) 041608.

[9] N.V. Priezjev, Molecular diffusion and slip boundary conditions at smooth surfaces with periodic and random nanoscale textures, J. Chem. Phys. 135 (2011) 204704.

[10] H. Hu, D. Wang, F. Ren, L. Bao, N.V. Priezjev, J. Wen, A comparative analysis of the effective and local slip lengths for liquid flows over a trapped nanobubble, Int. J. Multiph. Flow 104 (2018) 166.

[11] L. Bao, N.V. Priezjev, H. Hu, The local slip length and flow fields over nanostructured superhydrophobic surfaces, Int. J. Multiph. Flow 126 (2020) 103258.

[12] J. Servantie, M. Muller, Statics and dynamics of a cylindrical droplet under an external body force, J. Chem. Phys. 128 (2008) 014709.

[13] T. Koishi, K. Yasuoka, S. Fujikawa, T. Ebisuzaki, X.C. Zeng, Coexistence and transition between Cassie and Wenzel state on pillared hydrophobic surface, Proc. Natl. Acad. Sci. U.S.A. 106 (2009) 8435.

[14] X. Yong, L.T. Zhang, Nanoscale wetting on groove-patterned surfaces, Langmuir 25 (2009) 5045.

[15] Q. Yuan, Y.-P. Zhao, Wetting on flexible hydrophilic pillar-arrays, Sci. Rep. 3 (2013) 1944.

[16] S. Khan, J.K. Singh, Wetting transition of nanodroplets of water on textured surfaces: a molecular dynamics study, Mol. Simul. 40 (2014) 458.

[17] X.M. Xu, G. Vereecke, C. Chen, G. Pourtois, S. Armini, N. Verellen, W.-K. Tsai, D.-W. Kim, E. Lee, C.-Y. Lin, P.V. Dorpe, H. Struyf, F. Holsteyns, V. Moshchalkov, J. Indekeu, S. De Gendt, Capturing wetting states in nanopatterned silicon, ACS Nano 8 (2014) 885.

[18] D. Niu, G.H. Tang, Static and dynamic behavior of water droplet on solid surfaces with pillar-type nanostructures from molecular dynamics simulation, Int. J. Heat Mass Transf. 79 (2014) 647.

[19] H.-W. Pei, H. Liu, Z.-Y. Lu, Y.-L. Zhu, Tuning surface wettability by designing hairy structures, Phys. Rev. E 91 (2015) 020401(R).

[20] Q. Yuan, Y.-P. Zhao, Statics and dynamics of electrowetting on pillar-arrayed surfaces at the nanoscale, Nanoscale 7 (2015) 2561.

[21] J. Wang, S. Chen, D. Chen, Spontaneous transition of a water droplet from the Wenzel state to the Cassie state: a molecular dynamics simulation study, Phys. Chem. Chem. Phys. 17 (2015) 30533.

[22] A.M. Miqdad, S. Datta, A.K. Das, P.K. Das, Effect of electrostatic incitation on the wetting mode of a nano-drop over a pillar-arrayed surface, RSC Adv. 6 (2016) 110127.

[23] W. Xu, Z. Lan, B.L. Peng, R.F. Wen, X.H. Ma, Effect of nano structures on the nucleus wetting modes during water vapour condensation: from individual groove to nano-array surface, RSC Adv. 6 (2016) 7923.

[24] C.-C. Chang, Y.-J. Sheng, H.-K. Tsao, Wetting hysteresis of nanodrops on nanorough surfaces, Phys. Rev. E 94 (2016) 042807.

[25] J. Yan, K. Yang, X. Zhang, J. Zhao, Analysis of impact phenomenon on superhydrophobic surfaces based on molecular dynamics simulation, Comput. Mater. Sci. 134 (2017) 8.

[26] T.-H. Yen, Investigating the effects of wettability and gaseous nanobubbles on roughened wall-fluid interface using molecular dynamics simulation, Mol. Simul. 43 (2017) 1.

[27] H. Li, T. Yan, K.A. Fichthorn, S. Yu, Dynamic contact angles and mechanisms of motion of water droplets moving on nano-pillared superhydrophobic surfaces: a molecular dynamics simulation study, Langmuir 34 (2018) 9917.

[28] A.F.W. Smith, K. Mahelona, S.C. Hendy, Rolling and slipping of droplets on superhydrophobic surfaces, Phys. Rev. E 98 (2018) 033113.

[29] X. Geng, X. Yu, L. Bao, N.V. Priezjev, Y. Lu, Directed transport of liquid droplets on vibrating substrates with asymmetric corrugations and patterned wettability: a dissipative particle dynamics study, Mol. Simul. 46 (2020) 33.

[30] M.P. Allen, D.J. Tildesley, Computer Simulation of Liquids, Clarendon, Oxford, 1987.

[31] S.J. Plimpton, Fast parallel algorithms for short–range molecular dynamics, J.

Comput. Phys. 117 (1995) 1.

[32] K. Kremer, G.S. Grest, Dynamics of entangled linear polymer melts: a molecular dynamics simulation, J. Chem. Phys. 92 (1990) 5057.

[33] A. Tuteja, W. Choi, M. Ma, J.M. Mabry, S.A. Mazzella, G.C. Rutledge, G.H. McKinley, R.E. Cohen, Designing superoleophobic surfaces, Science 318

(2007) 1618.

[34] B. Bhattarai, N.V. Priezjev, Wetting properties of structured interfaces composed of surface-attached spherical nanoparticles, Comput. Mater. Sci. 143 (2018) 497.

[35] D.R. Heine, G.S. Grest, E.B. Webb, Spreading dynamics of polymer nanodroplets, Phys. Rev. E 68 (2003) 061603.